

# Local-Global Self-Supervised Visual Representation Learning

Ali Javidani\*, Mohammad Amin Sadeghi\*,\*\*, Babak Nadjar Araabi\*

\* Department of Electrical and Computer Engineering, University of Tehran, Tehran, Iran

\*\* Qatar Computing Research Institute, Doha, Qatar

**Abstract-** Self-supervised representation learning methods mainly focus on image-level instance discrimination. This study explores the potential benefits of incorporating patch-level discrimination into existing methods to enhance the quality of learned representations by simultaneously looking at local and global visual features. Towards this idea, we present a straightforward yet effective patch-matching algorithm that can find the corresponding patches across the augmented views of an image. The augmented views are subsequently fed into a self-supervised learning framework employing Vision Transformer (ViT) as its backbone. The result is the generation of both image-level and patch-level representations. Leveraging the proposed patch-matching algorithm, the model minimizes the representation distance between not only the CLS tokens but also the corresponding patches. As a result, the model gains a more comprehensive understanding of both the entirety of the image as well as its finer details. We pretrain the proposed method on small, medium, and large-scale datasets. It is shown that our approach could outperform state-of-the-art image-level representation learning methods on both image classification and downstream tasks.

**Index Terms-** Self-Supervised Learning; Visual Representations; Local-Global Representation Learning; Patch-Wise Representation Learning; Vision Transformer (ViT)

## 1. Introduction

Self-supervised representation learning growth was coupled with the appearance of instance discrimination. Instance discrimination has gained considerable attention during the last few years [1-10]. It behaves the samples in a mini-batch as separate classes. As a result, their representations are pushed away from each other. SimCLR [9] and MoCo [8] are among the two famous frameworks that could benefit from it. However, instance discrimination has its downsides. Firstly, the assumption of different classes for every sample in the mini-batch is not necessarily correct. This is because two or more samples in a mini-batch can imply the same concept and thus have the same labels. Secondly, pushing away the representations for every sample requires  $O(n^2)$  time complexity which hardens the training process. Thirdly, low-level features which contribute mostly to the details of an image are not captured.

Many works in the literature address the first and second problems. Clustering-based methods aim to tackle the first problem [11-15]. SwAV [14], PCL [13], and oBoW [11] by integrating online clustering as one of the steps in representation learning, could surge the performance of contrastive methods. Non-contrastive methods focus on avoiding degenerate solutions without pushing away the representations of every sample in the batch [16-24]. Their training speed has been boosted in comparison with contrastive methods. BYOL [23], SimSiam [20], and DINO [21] are examples of methods in this category. However, little research has been conducted to address the third problem [25, 26]. Most of the existing papers usually work on image-level features. Considering image-level features has led the machine to comprehend the overall concept of the image. However, some details that can play a significant role in determining the label of the image, may be disregarded. As a result, this area still seems to be open.

The main focus of our approach in this paper is to take a step towards a better understanding of the details of images when training in the self-supervised learning fashion. This is done by regulating the consistency loss for not only the augmented images but also the local regions, e.g., patches, inside the augmented variants. The latter results in generating additional loss terms which can guide the model to understand the details of images more prominently. Our main contributions to this work are as follows:

- Develop a simple yet effective patch-matching algorithm that is highly useful in self-supervised learning frameworks
- Introduce a novel inductive bias for training self-supervised models
- Propose a patch-wise self-supervised visual representation learning framework
- Compare the proposed method with other approaches, achieving state-of-the-art results on small, medium, and large-scale datasets

Our work is different from the literature on patch-wise self-supervised representation learning [25-27]. In SelfPatch the invariance constraint is enforced against each patch and its neighbors [25]. However, in some cases, adjacent patches may not share the same concept. In addition, it cannot help the machine to distinguish between different parts of an object. In contrast, our method, by pulling

the same object parts’ representations across the augmented images, guides the model to learn them effectively. In EsViT a multi-stage architecture with sparse self-attention is proposed [26]. Then, for capturing fine-grained features, a region-matching pretraining task is done. The region-matching task for each patch is done by finding the patch with the highest cosine similarity score. This approach has two main drawbacks. First, there is no guarantee that the most relevant patch is discovered by calculating the cosine similarity. Second, this process requires  $O(T^2)$  time complexity (where  $T$  is the number of patches) to find relevant patches. Thanks to the proposed patch-matching algorithm, our method does not suffer from either of the mentioned limitations. It finds the most relevant patch in  $O(1)$ . In [27], the assumption is to push away the representations of two local views of the same image as they might contain dissimilar content. However, this assumption may not always be true. In contrast, our technique identifies corresponding local regions across augmented views and minimizes the distance between their representations.

The rest of the paper is organized as follows. In section 2, the works related to our approach are reviewed. Section 3 explains the proposed method and the theory behind that extensively. In section 4, the results of our method and a comparison with the state-of-the-art methods on various datasets are reported. In section 5, discussions on the effects of the parameters related to our method are debated.

## 2. Related Works: Self-Supervised Representation Learning

### 2.1 Contrastive Methods

SimCLR stands out as the first and one of the most successful approaches that is based on contrastive loss [9]. It operates by extracting two distinct augmentations of each image within a mini-batch and subsequently performs instance classification, aiming to make the representations of augmented images from the same source image close while keeping representations from different images apart. SimCLR was extended to SimCLR-v2 [28], which employed massive task-agnostic unlabeled data for pre-training network weights and fine-tuning with labeled data. The model's scalability and performance depend on the mini-batch size that presents memory challenges. MoCo introduced a solution with separate query and key branches, allowing gradients from contrastive loss to backpropagate only through the query branch [8]. MoCo-v2 achieved even better results by using multiple queries [29], and Moco-v3 improved stability using ViT as a backbone [30]. Another method, Contrastive Predictive Coding (CPC), aimed to detect anomalies while learning self-supervised representations by predicting future data in latent space with probabilistic contrastive loss, emphasizing the capture of highly informative content for prediction [10]. Furthermore, Self-Distilled Self-Supervised Learning (SDSSL) was developed in which intermediate representations learn from the representation of the ultimate layer of the network through a self-distillation process [31].

Some works focused on boosting contrastive learning performance by selecting harder negative samples. In [7], the authors proposed hard negative mixing strategies at the feature level to generate synthetic samples. In [32], the mutual information between views is reduced to learn effective views. In a similar work, the ContrastiveCrop framework is proposed in which object localization is applied to craft better contrastive views [33]. Authors in NNCLR [4] claim that by finding the nearest samples to the anchor and treating them as positives, they could enhance the performance of contrastive learning. In [1, 2], different strategies for selecting difficult negative samples are proposed. Another work addresses this issue by generating hard negative examples [34]. A recent work identifies false negatives in the mini-batch and proposes cancellation and attraction strategies towards them to utilize their related information effectively [35]. In addition, in TMCT, a third network with momentum is used to provide the targets for the final model learning [36]. There also exist some works that investigated the applications of contrastive learning in different domains such as facial recognition [37] and animal detection [38].

### 2.2 Clustering-based Methods

Instance discrimination has demonstrated favorable performance enhancements within the domain of self-supervised representation learning. However, this methodology treats images from the same class as distinct instances, resulting in the divergence of their embeddings. In practical terms, when two images of the same class coexist within the same mini-batch, the applied loss function compels their representations, which is undesirable. To mitigate the contrastive learning limitation, some studies have integrated clustering into the overall framework [11-15]. As a first attempt, in Deep Embedded Clustering (DEC) a general framework was proposed in which an autoencoder is trained and, at the same time, the representations in the latent space are clustered [39]. Caron *et al.* trained a Convolutional Neural Network to extract features from the input and by performing clustering, they provided pseudo-labels for the network to be trained properly [15].

More recent research has combined contrastive learning and clustering to achieve superior results. In one instance, authors in [14], explored clustering with the Sinkhorn-Knopp transform after feature extraction from augmented images, specifying a predetermined number of clusters and assigning image representations to prototypes. Another approach, Prototypical Contrastive Learning (PCL), introduced prototypes as centroids for clusters of similar images, with each image assigned to multiple prototypes of varying granularity [13]. The training aimed to bring image embeddings closer to associated prototypes by minimizing a ProtoNCE loss function. In a

similar work, the OBoW method aimed to predict visual words constructed from original images using augmented versions, utilizing a teacher-student network structure where the teacher branch provided visual words and the student branch learned representations with momentum-based updates [11]. In the MCVT framework, cluster-based and info-based contrastive losses were combined to capture high-level and low-level features respectively [40]. In addition, the authors in [41], proposed Self-Supervised Pyramid Representation Learning (SS-PRL) to generate pyramid representations at the patch level by training appropriate prototypes. This framework also incorporates supplementary learners to analyze and establish connections between the inherent semantic information present within an image.

### 2.3 Non-Contrastive Methods

In contrast to contrastive learning, which considers both negative and positive pairs, in non-contrastive learning, the focus is solely on positive samples. An example of a non-contrastive approach is BYOL (Bootstrap Your Own Latent) [23]. BYOL extracts two sets of views from an image and passes them through encoders, with the target encoder being an exponential moving average of the online encoder. The loss is computed as the mean squared error between the online and target encoders. An extension of BYOL, MYOW, takes a different approach by using two nearby distinct samples instead of two different augmentations of the same image [22]. This results in significant performance improvements over BYOL. DINO utilizes self-distillation and involves both a teacher and student network adopting the Vision Transformer (ViT) architecture [21]. Notably, the teacher network employs momentum, maintaining exponentially weighted average weights of the student network. Additional centering and sharpening modules are used to prevent trivial solutions. Following BYOL’s success, the authors in MSBReg, by combining three loss terms capturing information from multiple sources, could further increase the performance [42]. Furthermore, SimSiam demonstrates remarkable performance even without auxiliary structures like negative samples, clustering, or moving averages [20]. This makes it computationally efficient and results in outperforming other self-supervised networks, such as SimCLR and BYOL, particularly in terms of training with smaller batch sizes.

A recent category in non-contrastive approaches aims to maximize the information content within representation vectors while preventing the issue of representation collapse, as discussed in prior studies [43]. These methods introduce specific constraints into their objective functions to deter the representations from converging into a constant vector. In one instance, this is achieved by performing whitening on the latent space obtained from processing diverse augmentations of the same image [19]. In another approach, the empirical cross-correlation matrix is computed and optimized to resemble the identity matrix, a framework known as Barlow Twins, to reduce redundancy among inputs [18]. Complementing this work, authors in [16] introduced an additional loss term that elevates the variance among images within the mini-batch above a predefined threshold, yielding more robust outcomes. Further exploration by Zhang *et al.* involved randomly grouping feature dimensions and comparing them with basis norms [44]. Wang *et al.* proposed TWIST, which enforces similarity in the class distributions of two augmented images by introducing a constraint on mutual information maximization in the cost function to prevent collapse [45]. Additionally in Self-Classifier, modifications to the standard cross-entropy characterized by a uniform prior assumption on predicted labels led to enhanced results [46].

## 3. Proposed Local-Global Representation Learning

### 3.1 An Explanation of DINO and Its Limitation

The recent self-supervised framework DINO, with the aid of knowledge distillation, could utilize the power of Vision Transformers (ViTs) for the self-supervised representation learning problem [21]. In this framework, by performing various kinds of augmentations, the global and local crops of an original image are extracted. The global crops pass through the teacher and both the global and local crops pass through the student network. The idea is to pull representations resulting from the outputs of these two networks. As a result, the CLS embedding, which is the representation of the whole image, is extracted for each augmented image. Then, the cross-entropy loss between the outputs of student and teacher networks is computed to match the representation of the local image with the representation of the global variant.

In this framework, the emphasis is placed solely on the CLS tokens, serving as representatives of the entire input image, while tokens associated with image patches are disregarded. Essentially, the model captures image-level representations while neglecting patch-level representations. While it is shown that the image-level representation constraint leads the model to learn a meaningful representation, this constraint may not be sufficient for acquiring an exhaustive representation space. For instance, when an image encompasses multiple objects, matching representations of the entire image across augmented views may lead to confusion regarding the primary focus of the image. However, introducing specific constraints, such as ensuring consistency in representations of local regions, could enhance the model’s understanding of image components. This approach facilitates a discernible differentiation between object representations. Even if the image contains only a single object, by imposing additional specific restrictions, the model is anticipated to develop an enhanced understanding of the various components of the object. For example, if the image depicts a dog, by pulling representations of the dog’s head in the augmented images, the model can distinguish between the head and other parts of the dog more effectively.

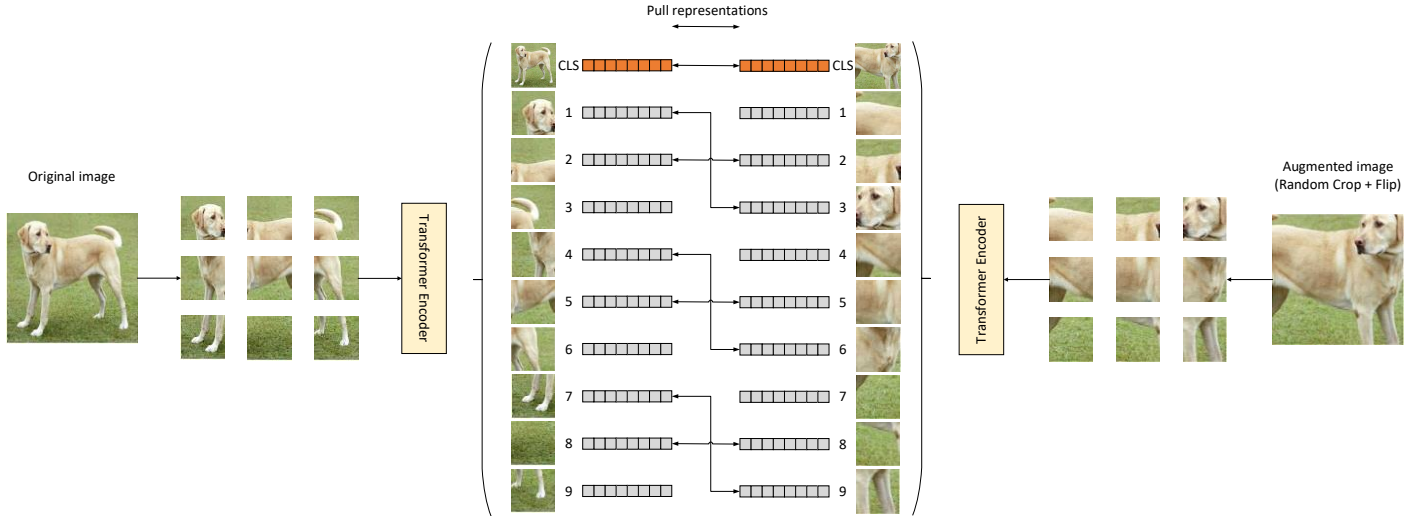


Figure 1 An existing dog image is augmented via random crop and flip operations. Both the original and augmented images are fed to the Vision Transformer (ViT) encoders. The ViT encoder splits the image into equally sized patches and extracts representations for both the entire image (CLS tokens) and each patch. Our idea is to minimize the distance between CLS tokens as well as corresponding patch tokens across views. Pulling the CLS tokens gives the model an idea of the entire object in the image; while minimizing the distance between the patch tokens guides the model toward a better understanding of the details of the object.

### 3.2 Proposed Idea: Local-Global Matching

Our key idea is to capture local information inside the image patches and use it alongside the global information to train the model more effectively. One approach to acquiring local information is to match correspondent patches across augmented images which leads to generating additional loss terms. We think these supplemental loss terms can serve as valuable inductive biases for the model facilitating the capture of abstraction levels with finer granularities. This is in contrast to the original DINO, where such loss terms were entirely disregarded. Consequently, our approach empowers the model not only to comprehend the overarching concepts within an image but also to develop a profound understanding of its constituent details.

Figure 1 illustrates the overall idea of this paper using transformer encoders. Vision Transformers (ViTs) divide the image into patches and output an embedding vector for each patch. This property simplifies the implementation of the proposed idea enormously. The proposed framework is as follows: The original image is augmented. The original and augmented images are fed to the Vision Transformer encoder network. The encoder network yields CLS tokens and tokens related to the patches inside the images. Then the loss is calculated by matching both the CLS tokens and the correspondent patches. This idea, of course, requires a patch-matching algorithm, that finds the corresponding patches across augmented crops, which will be discussed in the next section.

### 3.3 Patch-Matching Algorithm

In this work, we followed DINO’s settings in which there exist two network streams teacher and student. The global crops, which consist of more than 50% of the original image, are fed to the teacher network, and the global crops plus local crops are fed to the student network. Local crops contain less than 50% of the image. These crops result from performing data augmentation operators such as random resize crop, horizontal flip, and color jittering (including random grayscale, and playing with brightness, contrast, saturation, and hue). They are resized to  $96^2$  for the local and  $224^2$  for the global crops. Among these augmentations, random crop and horizontal flip operators have the most significant impact on the patch locations. Other augmentation operators such as color jittering, Gaussian noise or blurring, sobel filtering, etc. do not cause any changes in the patch locations.

Figure 2 demonstrates the patch-matching algorithm when performing random crop on the original image. To find the patch correspondences across the global and local crops, it is necessary to find the intersection area between the global and local crops. Because if the intersection area is empty, there would not be any correspondent patches (only the CLS tokens should match together in this case). To find the intersection area, we need to know which parts of the original image have been cropped. By taking the intersection between the start-to-end pixel intervals of local and global crops, the intersection area (green rectangle in Figure 2) is determined. This area contributes to different patches for the local and global crops. (It may not cover the whole patch at the edges of the rectangle, however, we assumed that if it contains more than 50% of both the width and height of a patch, that patch will be included).

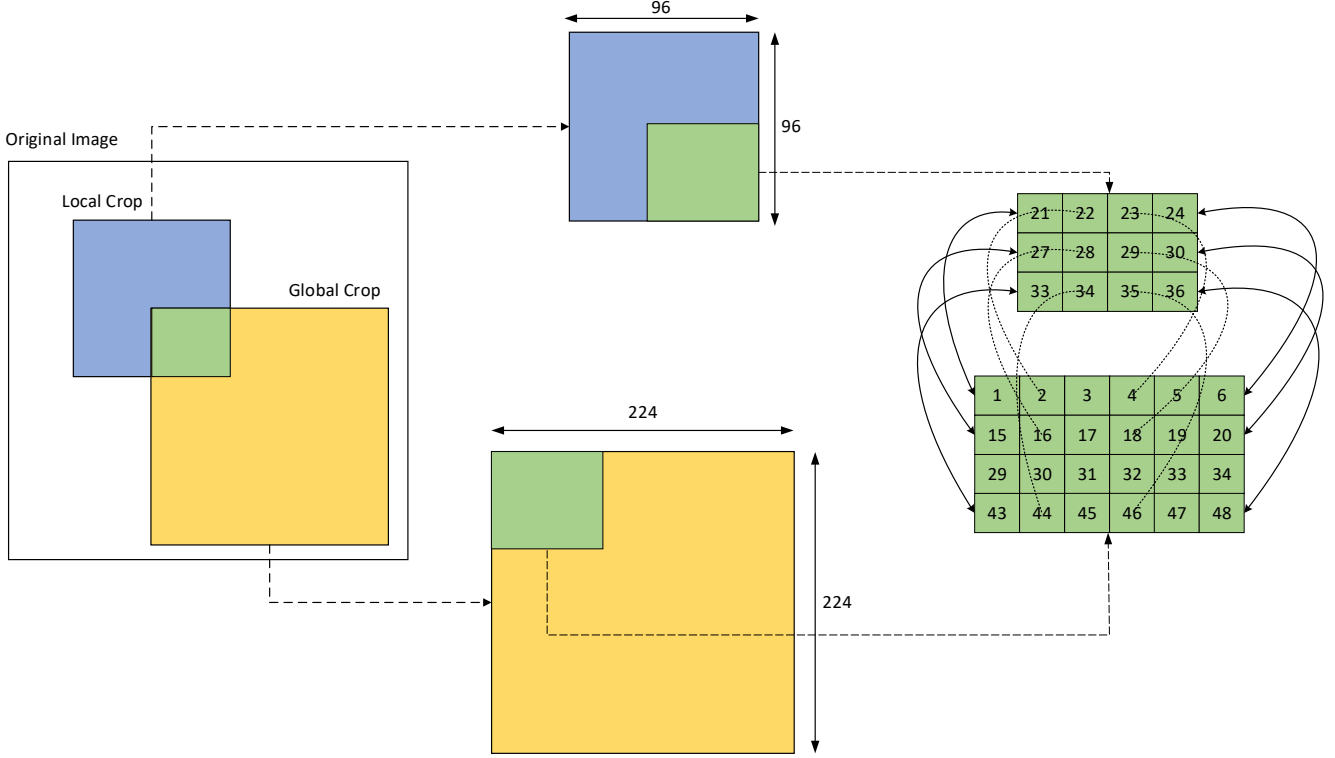


Figure 2 The original image is augmented in two ways local and global crops. The local crop (blue rectangle) contains less than 50% of the original image while the global crop (yellow rectangle) contains more than 50% of it. Then, local and global crops are resized to  $96^2$  and  $224^2$  respectively. To find the corresponding patches across the local and global crops, the intersection area (green rectangle) is determined. The intersection area contains individual patches for the local and global crops. In this example, some patches between 21 to 36 are present for the local crop and the global crop contains some patches between 1 to 48. To find corresponding patches along the rows, starting from the first row, we only select rows with an interval that results from taking the floor of dividing the number of rows in the global crop by the number of rows in the local crop. Here, the first, second, and fourth rows are selected. The same happens for columns as well. In this example, the first, second, fourth, and sixth columns are selected.

In our patch-matching algorithm, since the local crop usually contains a lesser number of patches w.r.t. the global variant, only some of the global crop patches can be matched to the local crop patches. To find those patches along the rows, starting from the first row, we only select rows with a specified interval. This interval results from taking the floor of dividing the number of rows in the global crop by the number of rows in the local crop. The simple intuition behind it is that we want to try to distribute the local crop patches evenly into the global crop. The same algorithm happens for the columns as well. When the horizontal flip is done on either local crop or global crop or both, the only difference is that the sequence order of patches in that image is reversed. The result of performing our patch-matching algorithm on a real image is illustrated in Figure 3.

### 3.4 Loss Function Setup

We followed the DINO's structure which benefits from knowledge distillation to train the whole framework effectively. The teacher network has not been previously trained and is being trained with the student simultaneously. In the original DINO, various update rules for the teacher have been investigated. The one that fits well in this framework is to use the Exponential Moving Average (EMA) to update teacher parameters. The update rule is as follows:  $\theta_t \leftarrow \lambda\theta_t + (1 - \lambda)\theta_s$  where  $\theta_t$ ,  $\theta_s$  denote the parameters of the teacher and student networks respectively, and  $\lambda$  follows a cosine schedule. Also, to avoid collapse the centering and sharpening operators have been used. By feeding an image to the network, the probability distribution  $P$  results due to the softmax function as the ultimate layer:

$P_s(x)^i = \frac{\exp(\theta_s(x)^i/\tau_s)}{\sum_{k=1}^K \exp(\theta_s(x)^k/\tau_s)}$  where  $i$  denotes the  $i^{th}$  dimension of the distribution,  $\tau_s$  is the temperature parameter of the student controlling the sharpness of the output distribution. The teacher network shares the same structure with the difference that the centering operator  $C$  is also involved:  $P_t(x)^i = \frac{\exp((\theta_t(x)^i - C)/\tau_t)}{\sum_{k=1}^K \exp((\theta_t(x)^k - C)/\tau_t)}$  where  $C$  is the average of samples inside the batch.

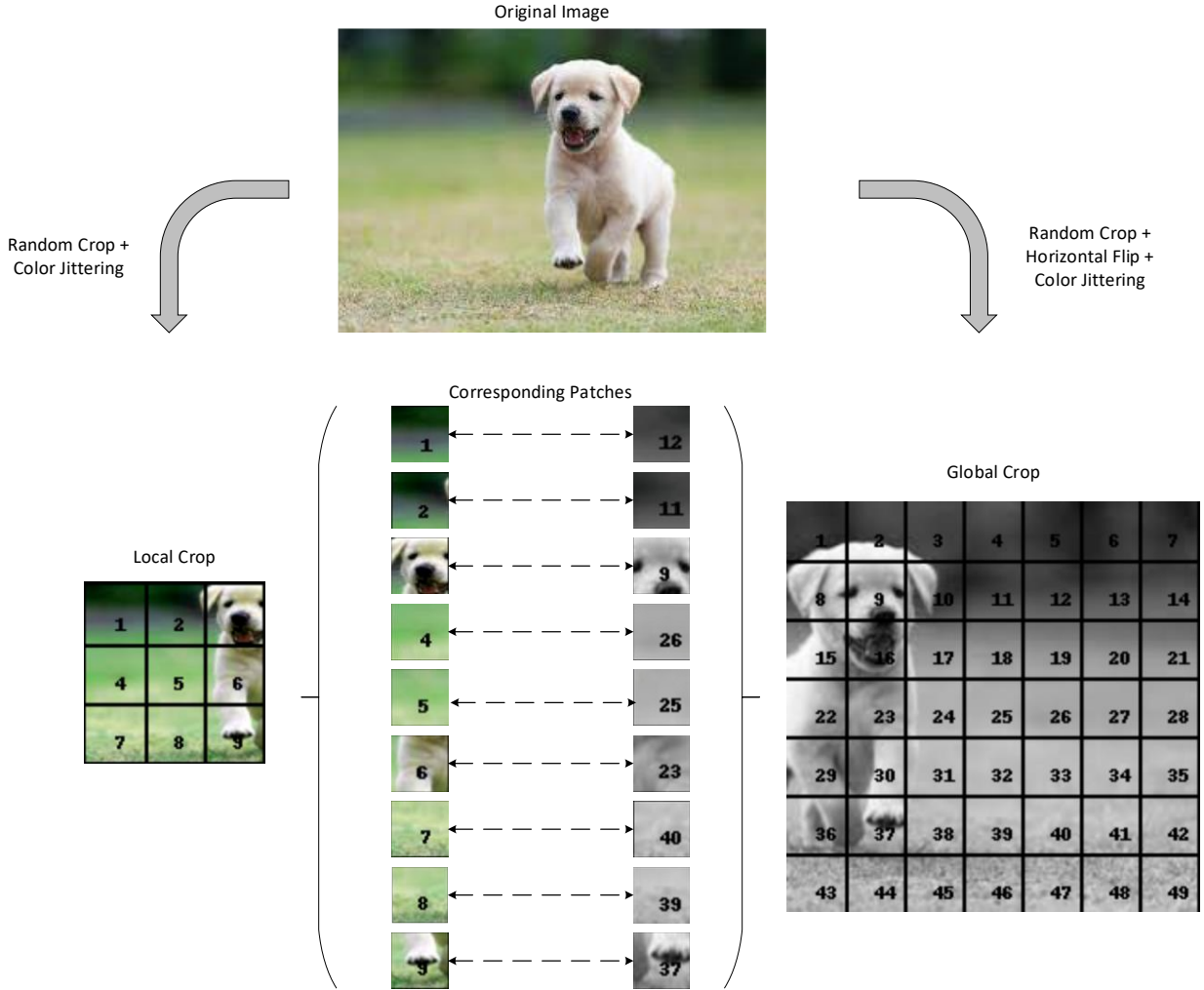


Figure 3 The result of performing the proposed patch-matching algorithm on a real image. The local crop results by performing random crop and color jittering on the original image, while the global includes these operators as well as horizontal flip. In this example, the global crop contains the whole local crop. As a result, all patches inside the local crop are matched with their corresponding patches in the global variant. For instance, patch #3 of the local is matched with patch #9 of the global where both contain the dog's face. As another example, patch #9 of the local is matched with patch #37 of the global, where both contain dog's hands.

If  $x_i$  is the  $i^{th}$  image in the batch, by performing augmentations on that,  $x_i^{g(j)}, x_i^{l(j)}$  result which are the  $j^{th}$  global and local crops of  $x_i$  respectively. In the original DINO setting, 2 global and 8 local crops are extracted. These 2 global crops are passed through both the teacher and student networks. The results are  $g_i^j = P_t(x_i^{g(j)}), j = 1, 2$  and  $gs_i^j = P_s(x_i^{g(j)}), j = 1, 2$  respectively. The 8 local crops are only fed to the student network where the results are  $ls_i^j = P_s(x_i^{l(j)}), j = 1, 2, \dots, 8$ . Hence the outputs of the student network are  $l_i^j = [gs_i^1, gs_i^2, ls_i^1, ls_i^2, \dots, ls_i^8]$ ; where the first two elements are the results of feeding global crops and the eight remaining are from feeding local crops. Then, the loss between the outputs of teacher and student is calculated using the cross-entropy loss formula  $H(a, b) = -a \log(b)$ .

In the original DINO loss function, the cross entropy between the CLS representations (token 0) of the outputs of teacher and student are calculated. Two cases are excluded from the loss calculations. Those are when  $i = j = 1$  and  $i = j = 2$ . The reason is because in both cases, the student and teacher have been operated on the same view. The mentioned operation is repeated for every image in the batch. The final loss is the average of terms calculated.

$$Original \ DINO \ Loss = \frac{\sum_{b=1}^{batch-size} \sum_{i=1}^2 \sum_{j=1, j \neq i}^{10} H(g_b^i[0], l_b^j[0])}{batch-size \times 18}$$

In the patch-wise DINO loss (mean), the same operations are done with the difference that for every global and local crop, the correspondent patches have been calculated and stored in  $g_b^i$  and  $l_b^j$ . Hence the cross-entropy between all the matched patches (including CLS token plus other tokens) are calculated. The final loss is the average between those terms.

$$\text{Patch-Wise Mean Loss} = \frac{\sum_{b=1}^{\text{batch-size}} \sum_{i=1}^2 \sum_{j=1, j \neq i}^{10} (\sum_{p=0}^{\#(\text{matched-patches})-1} H(g_b^i[p], l_b^j[p]) / \#(\text{matched-patches}))}{\text{batch-size} \times 18}$$

In the patch-wise sum loss, the only difference w.r.t. the patch-wise mean loss is that the final loss comes from the summation of the cross-entropy terms but is not divided by the number of matched patches.

$$\text{Patch-Wise Sum Loss} = \frac{\sum_{b=1}^{\text{batch-size}} \sum_{i=1}^2 \sum_{j=1, j \neq i}^{10} \sum_{p=0}^{\#(\text{matched-patches})-1} H(g_b^i[p], l_b^j[p])}{\text{batch-size} \times 18}$$

In both patch-wise mean loss and patch-wise sum loss, each cross-entropy term contributes to the final loss equally. However, in patch-wise  $\lambda$  loss, we differentiate between the CLS tokens and other tokens. This is done by giving the  $\lambda$  weight to the CLS tokens and  $1 - \lambda$  weight to others. In the ablation study section, various experiments have been done to investigate the effect of the  $\lambda$ .

$$\text{Patch-Wise Lambda } (\lambda) \text{ Loss} = \frac{\sum_{b=1}^{\text{batch-size}} \sum_{i=1}^2 \sum_{j=1, j \neq i}^{10} (\lambda \times H(g_b^i[0], l_b^j[0]) + (1 - \lambda) \times \left( \frac{\sum_{p=1}^{\#(\text{matched-patches})-1} H(g_b^i[p], l_b^j[p])}{\#(\text{matched-patches})-1} \right))}{\text{batch-size} \times 18}$$

A pseudo-code implementation is proposed in Algorithm 1 for better comprehension of the algorithm. The full implementation is also available on Github<sup>1</sup>.

Algorithm 1 Local-Global Self-Supervised Representation Learning Pseudocode in Python

```
# gs, gt: student and teacher networks
# C: center (K)
# tps, tpt: student and teacher temperatures
# l, m: network and center momentum rates
gt.params = gs.params

for b in loader: # load a minibatch b with n samples
    [b1, cropped_coords1, flipped1] = augment(b) # b1 random view, cropped_coords1 cropped area coordinates in b1, flipped1 is 1 if flipped else 0
    [b2, cropped_coords2, flipped2] = augment(b) # b2 random view, cropped_coords2 cropped area coordinates in b2, flipped2 is 1 if flipped else 0

    # find correspondent patches:
    correspondences = patch_matching([b1, cropped_coords1, flipped1], [b2, cropped_coords2, flipped2])

    t = gt(b1) # teacher output n x m x K => n samples in the batch - m number of patches+1 - K dimensions
    s = gs(b2) # student output n x m x K => n samples in the batch - m number of patches+1 - K dimensions

    # calculate loss:
    loss = H(t, s, correspondences)
    loss.backward() # back-propagate

def H(t, s, correspondences):
    t = t.detach() # stop gradient

    # Select Correspondent Patches:
    t_selected_patches = t[:, correspondences.selected_crop1_patches, :]
    s_selected_patches = s[:, correspondences.selected_crop2_patches, :]

    # Softmax student and teacher selected patches outputs:
    t_softmax = softmax((t_selected_patches - C) / tpt, dim=-1) # center + sharpen
    s_softmax = log_softmax(s_selected_patches / tps, dim=-1)

    # Calculate Loss:
    cross_entropy_loss = - t_softmax * s_softmax
    loss_tensor = torch.sum(cross_entropy_loss, dim=-1) # Summation over dimensions
    final_loss = loss_formula(loss_tensor) # loss_formula: Mean or Sum or Lambda (λ)
    return final_loss
```

<sup>1</sup> [https://github.com/alijavidani/Local\\_Global\\_Representation\\_Learning](https://github.com/alijavidani/Local_Global_Representation_Learning)

## 4. Results

### 4.1 Experimental Setup

#### 4.1.1 Datasets

The datasets used in this work are in common with related works in the literature. We have used three datasets Cifar10, ImageNet-100, and ImageNet-1K to pretrain our network. Cifar10 is a small-scale dataset that has 10 classes with images in  $32 \times 32$  resolutions. It has 60,000 images of which 50,000 are for training and 10,000 for validation. ImageNet-1K is an image dataset that aligns with the WordNet hierarchy. Each synset represents a meaningful concept and is associated with one or more words or word phrases. ImageNet’s primary goal is to offer an average of 1,000 curated images for each synset, all of which undergo quality control and human annotation. It encompasses 1000 object classes and comprises 1,281,167 training images, 50,000 validation images, and 100,000 test images. ImageNet-100 is a subset of the ImageNet-1K dataset that has 100 classes randomly selected. The dataset is well-balanced such that each class contains 1,300 training images and 50 validation images.

#### 4.1.2 Implementation Details

In order to find the patch correspondences across the global and local crops, it is necessary first to find the intersection area between the global and local crops. For that, it is needed to return the cropped area (start and end pixels for both the width and height), randomly chosen from the original image when performing random crop operation. These parameters are not returned by default in deep learning frameworks *TensorFlow* and *PyTorch*. As a result, we overwrote the original implementation of the method in PyTorch. By doing so, we could find the intersection area between each crop extracted from the original image.

When computing the loss function for samples in the mini-batch according to the proposed method, the initial step involves applying the patch-matching algorithm to each image in the batch. Subsequently, based on the matched patches, the cross-entropy loss between them is calculated and incorporated into the overall loss formula. However, this computation process is notably time-consuming. This contrasts with the original DINO framework, which exclusively matches CLS tokens without seeking matched patches. In our framework, the tokens that necessitate alignment differ for each instance in the batch, imposing an additional computational burden in terms of time and memory compared to DINO. To mitigate this, we introduced a simplifying bias into the algorithm. The bias mandates that all images in the batch undergo augmentation with similar parameters. Specifically, random crop and horizontal flip operations—two crucial parameters in image augmentation—are executed uniformly for images in the mini-batch by setting the same randomness seed for these operations across batch images. Since color jittering does not influence patch locations, it remains unaffected by setting the same random seed. Consequently, to identify matched patches for images within the batch, it is only necessary to find matched patches for one instance, and the outcomes can be generalized to other instances in the batch.

In this work, we followed DINO’s implementation details. The Adamw optimizer with batch sizes from 10 to 40 is used for different datasets. The learning rate undergoes a linear ramp-up phase in the initial 10 epochs until it reaches its base value. It decays based on a cosine schedule. Similarly, the weight decay follows a cosine schedule, transitioning from 0.04 to 0.4. The temperature parameter ( $\tau_s$ ) is set at 0.1, and a linear warm-up scheme is applied to the parameter  $\tau_t$ , transitioning from 0.04 to 0.07 for the initial 30 epochs.

### 4.2 Evaluation: Linear and KNN image classification

Like other self-supervised representation learning methods, the proposed method is pretrained on a dataset without considering its labels. Here, we pretrained our algorithm on three datasets Cifar10, ImageNet-100, and ImageNet-1K separately. In the next stage, the images of that dataset are fed to the pretrained network, and the features are extracted to classify those images. The classification is done in two manners: 1) Linear validation: an MLP layer is placed on top of the extracted features. Then, it will be trained to classify the images. 2) KNN validation: The features are extracted and frozen. The K-Nearest Neighbors (KNN) with  $K=10$  or  $20$  is performed on the resulting representations.

#### 4.2.1 Pretraining on Cifar10

Table 1 illustrates the results of validating the frozen features that come from pretraining the network for classifying the Cifar10 dataset after training for 200 epochs. As it is clear, the proposed method, with any loss function, outperforms the original DINO and other state-of-the-art methods both in linear validation and KNN validation. An interesting point is that our method (when using the mean loss function) could obtain more increase in comparison with DINO when doing KNN validation compared to when doing linear validation. To explain it more, by comparing the results of our method with DINO, (rows 3 and 9 in Table 1), the increase obtained in linear validation is +5.73%, while the increase that happened in KNN validation ( $K=10$ ) is +7.48%. This phenomenon ascertains that in the situation where there is no additional training phase (like KNN validation), the separability of the representations resulting from our method is higher than the original DINO.

Table 1 The comparison of our method and state-of-the-art methods when pretrained on Cifar10 for 200 epochs. The proposed method is trained with ViT-Base as the backbone. The experiments are done with various configurations for loss function (patch-wise mean, patch-wise sum, and patch-wise  $\lambda$ ), and patch size 16. Linear validation and KNN validation columns demonstrate the Cifar10 image classification accuracies. In all experiments, the proposed method could outperform existing approaches.

Pretraining Dataset	Method	Linear Validation	KNN Validation	
			(K=10)	(K=20)
Cifar10	SCLR [9]	86.54	82.81	82.11
	MoCov2 [29]	87.61	83.52	83.74
	DINO (ViT-Tiny/16) [21]	87.51	84.44	84.91
	BarlowT [18]	88.74	86.14	85.26
	OBoW [11]	88.81	87.64	86.17
	SwAV [14]	90.13	90.41	88.84
	BYOL [23]	90.41	89.32	90.87
	ARB [44]	92.19	91.75	91.46
	Ours (ViT-Base/16 + Mean)	93.24	<b>91.92</b>	<b>91.56</b>
	Ours (ViT-Base/16 + Sum)	92.54	90.13	90.01
Ours (ViT-Base/16 + $\lambda = 0.2$ )	<b>93.82</b>	91.42	91.31	

#### 4.2.2 Pretraining on ImageNet-100

Table 2 presents the results of the comparison of our method and other state-of-the-art approaches when pretrained on ImageNet-100 after training for 200 epochs. The proposed method with the patch-wise mean loss function and patch size 16 could outperform other state-of-the-art methods both in linear and KNN validations. More experiments with various backbone architectures ViT-Tiny, ViT-Small, and ViT-Base are done and reported in Table 3 to provide more visibility. One interesting point in Table 3 is that the linear validation improvements made by our method in comparison with DINO have been increased by enlarging the number of training parameters. To explain it more, when ViT-Tiny, ViT-Small, and ViT-Base are used as the backbone, the linear validation improvements of our method w.r.t the DINO are +3.44%, +3.52, and +4.58% each in order. This confirms that our method, due to the injected inductive biases through the learning process, has more capacity to learn the relations in comparison with the DINO.

Table 2 The results comparison of our method and state-of-the-art methods when pretrained on ImageNet-100 for 200 epochs. The proposed method is trained with ViT-Base as the backbone, patch-wise mean loss function, and patch size 16. Linear validation and KNN validation columns demonstrate the ImageNet-100 image classification accuracies. The proposed method could outperform existing approaches.

Pretraining Dataset	Method	Linear Validation	KNN Validation	
			(K=10)	(K=20)
ImageNet-100	SCLR [9]	71.72	55.64	55.92
	MoCov2 [29]	74.12	57.65	57.41
	OBoW [11]	75.29	58.43	58.74
	BarlowT [18]	76.91	58.48	58.32
	BYOL [23]	77.52	59.58	59.19
	SwAV [14]	77.68	61.51	61.74
	DINO (ViT-Base/16) [21]	78.22	68.58	68.84
	ARB [44]	79.48	73.51	73.87
	MSBReg [42]	81.56	74.51	75.12
	Ours (ViT-Base/16 + Mean)	<b>82.80</b>	<b>75.24</b>	<b>75.43</b>

Table 3 The results comparisons of our method and DINO when pretrained on ImageNet-100 for 200 epochs. Both methods are trained with ViT-Tiny, ViT-Small, and ViT-Base as the backbone. Patch-Wise Mean loss is used as the loss function for our method. Linear validation and KNN validation columns demonstrate the ImageNet-100 image classification accuracies. In all experiments, the proposed method could outperform the original DINO.

Pretraining Dataset	Method	Backbone	Patch size	Loss Function	Linear Validation	KNN Validation	
						(K=10)	(K=20)
ImageNet-100	DINO [21]	ViT-Tiny	16	-	58.08	51.84	52.74
	Ours	ViT-Tiny	16	Mean	<b>61.52</b>	<b>58.66</b>	<b>58.1</b>
	DINO [21]	ViT-Small	16	-	70.92	64.64	64.74
	Ours	ViT-Small	16	Mean	<b>74.44</b>	<b>67.92</b>	<b>68.16</b>
	DINO [21]	ViT-Base	16	-	78.22	68.58	68.84
	Ours	ViT-Base	16	Mean	<b>82.80</b>	<b>75.24</b>	<b>75.43</b>

### 4.2.3 Pretraining on ImageNet-1K

We pretrained the proposed method with ViT-Base, patch size 16, and the patch-wise mean loss function on ImageNet-1K for 50 epochs. The linear and KNN validation results are reported in Table 4. As can be seen, the proposed method could successfully outperform other existing methods.

Table 4 The results comparison of our method and state-of-the-art methods when pretrained on ImageNet-1K for 50 epochs. The proposed method is trained with ViT-Base as the backbone, patch-wise mean loss function, and patch size 16. Linear validation and KNN validation columns demonstrate the ImageNet-1K image classification accuracies. The proposed method could outperform existing approaches.

Pretraining Dataset	Method	Linear Validation	KNN Validation	
			(K=10)	(K=20)
ImageNet-1K	SCLR [9]	60.06	52.81	51.16
	BarlowT [18]	61.02	58.71	56.59
	ARB [44]	62.05	63.46	62.51
	MoCov2 [29]	64.53	53.14	52.78
	OBoW [11]	68.76	58.49	57.13
	BYOL [23]	69.87	60.51	60.13
	SwAV [14]	70.84	62.49	61.19
	DINO (ViT-Base/16) [21]	71.46	64.55	64.34
	Ours (ViT-Base/16 + Mean)	<b>73.42</b>	<b>67.89</b>	<b>67.52</b>

### 4.3 Evaluation: Downstream Tasks

The resulting features can be applied in other image applications as well. In this work, two downstream tasks copy detection and image retrieval are selected to test the generalizability of the representations coming out from the pretrained networks.

#### 4.3.1 Copy Detection

This task is to recognize the distortions of types of insertions, blurring, printing, etc. To evaluate the performance of the methods, the mean Average Precision (mAP) is reported on the “strong” subset of the Copydays dataset. Two distinct image sets of 10k and 20k are required to run the task. The 10k set is for distractor images, and the 20k set is for learning the parameters of the whitening operator. When evaluating the networks pretrained on Cifar10 and ImageNet-100, both image sets are randomly sampled from the ImageNet dataset excluding the images contained in the ImageNet-100. While, when evaluating the network pretrained on ImageNet-1K, the whole ImageNet-1K was used to train those parameters. Table 5 compares the results of the original DINO and ours when pretrained on Cifar10, ImageNet-100, and ImageNet-1K respectively. The proposed method could outperform DINO.

#### 4.3.2 Image Retrieval

The revisited Oxford and Paris datasets were used for the image retrieval task. They both contain 3 splits Easy (E), Medium (M), and Hard (H). We report the mean Average Precision (mAP) on Medium and Hard splits, following DINO’s tradition [21]. After pretraining with either DINO or the proposed method, the images of the mentioned datasets were fed to the network. Then, the features are extracted and frozen. Finally, the KNN classifier is applied to retrieve the most relevant images. The mAPs for two datasets are reported when pretrained on Cifar10, ImageNet-100, and ImageNet-1K in Table 5 respectively. As can be seen, using the proposed method with mean loss function outperforms the original DINO in both Medium and Hard splits in both datasets Oxford and Paris.

Table 5 The comparison of downstream tasks results between our method and DINO, when pretrained on Cifar10, ImageNet-100, and ImageNet-1K. The downstream tasks are copy detection and image retrieval. The mAP is reported on the “strong” subset of the copydays (copy detection), and Oxford and Paris (image retrieval) datasets. The proposed method could outperform DINO in both tasks.

Pretraining Dataset	Method	Backbone	Patch size	Loss Function	Copy Detection	Image Retrieval	
						Oxford	Paris
Cifar10	DINO [21]	ViT-Tiny	16	-	0.574	M: 6.33, H: 1.57	M: 17.07, H: 4.58
Cifar10	Ours	ViT-Tiny	16	Mean	0.591	M: 8.34, H: 1.63	M: 21.18, H: 5.11
ImageNet-100	DINO [21]	ViT-Tiny	16	-	0.645	M: 11.87, H: 2.73	M: 20.13, H: 5.04
ImageNet-100	Ours	ViT-Tiny	16	Mean	0.647	M: 12.22, H: 2.76	M: 24.21, H: 7.57
ImageNet-1K	DINO [21]	ViT-Base	16	-	0.707	M: 25.85, H: 9.13	M: 54.88, H: 27.84
ImageNet-1K	Ours	ViT-Base	16	Mean	0.747	M: 28.66, H: 9.17	M: 58.11, H: 29.71

## 5. Discussions

In this section, we explore the effect of the patch size, backbone architectures, proposed loss functions, and lambda value parameters in our method. The final linear and KNN validation accuracies and downstream task results are evaluated.

### 5.1 Effect of Patch Size

The impact of the patch size parameter is evident in Table 6 (rows 2 and 4) and Table 8 (last two rows). For instance, in Table 6, when pretraining on Cifar10, a reduction in the patch size from 32 to 16, while maintaining other parameters constant, resulted in a notable increase of +2.37% in linear validation accuracy and +5.17% in KNN validation accuracy. However, in Table 8, pretraining on ImageNet-100 and reducing the patch size led to a decrease of -4.27% in linear validation accuracy and -5.36% in KNN validation accuracy. This decline is attributed to potential overfitting, wherein an excessive reduction in patch size generates an abundance of patch correspondences, each serving as a constraint during model training. The presence of numerous constraints may induce overfitting, thereby compromising model performance. Consequently, a reduction in patch size improves model performance up to a certain threshold; beyond this point, however, further reduction may induce overfitting.

### 5.2 Effect of Backbone Architecture

Table 8 presents the results of our method when pretrained on ImageNet-100 with various backbone architectures while fixing other parameters as constant. The backbone architectures ViT-Tiny, ViT-Small, and ViT-Base are utilized which have 5.8, 22.2, and 86 million parameters respectively. By increasing the training parameters, the opportunity is given to the model to better fit the real representation manifold. Hence, better classification accuracies have been achieved when backbones with more training parameters have been used. However, it is also important to consider that sometimes more training parameters result in overfitting to the data. This happens when the model has used its capacity and there is no more space to learn. In our case, since a significant increase has occurred when going from ViT-Small to ViT-Base (+8.36%), it can be deduced that there is more space to learn and overfitting is an unlikely situation.

### 5.3 Effect of the Loss Function

Table 6 and Table 7 provide reports to compare the results of integrating the proposed loss functions when pretrained on Cifar10. A general point is that there is not much difference between employing different loss functions. Utilizing each of them can result in prominent results either in linear and KNN classification or on downstream tasks. From a practical point of view, the property of not being dependent on the loss function seems critical. Changing the loss function in different situations can increase the performance in the desirable metric, while at the same time will not downgrade the performance of other metrics significantly. However, utilizing the patch-wise mean loss function seems to lead to superior results in KNN classification and image retrieval task (both datasets Oxford and Paris). In addition, when using the lambda loss function, some values of  $\lambda$  (e.g.,  $\lambda=0.5$  or  $0.2$  in Table 6) can lead to better linear validation accuracies compared to when using the mean loss function.

### 5.4 Effect of Lambda ( $\lambda$ ) value

An interesting point in Table 6 is that in the proposed method, when using the lambda loss function, the more the lambda value is decreased, the better performances are obtained. For example, when setting  $\lambda = 0.8$ , the effect of the CLS token in the overall loss value is 80% and the effect of other tokens is 20%. In this case, the linear validation is 76.52%. However, when setting  $\lambda = 0.2$ , the effect of the CLS token is only 20%, and the effect of other tokens is 80%. In this scenario, the linear validation has become 79.65%. This highlights the importance of considering patch representations concerning the CLS token. In fact, it verifies the main idea of this paper, which is learning from not only the whole image but also smaller patches inside the image. This point is valid when comparing the downstream tasks results in Table 7 as well. As it is clear, by decreasing the lambda value (until 0.2 for image retrieval and 0.5 for copy detection), the mAP values have been increased.

Table 6 The results comparison of our method with different configurations when pretrained on Cifar10. The proposed method is trained with ViT-Tiny as the backbone. The experiments are done with various configurations for loss function (patch-wise mean, sum, and  $\lambda$  with multiple values for  $\lambda$ ), and patch sizes 32 and 16. Linear validation and KNN validation columns demonstrate the Cifar10 image classification accuracies.

Pretraining Dataset	Method	Backbone	Patch size	Loss Function	Linear Validation	KNN Validation	
						(K=10)	(K=20)
Cifar10	DINO [21]	ViT-Tiny	32	-	71.05	72.19	72.67
	Ours	ViT-Tiny	32	Mean	<b>75.73</b>	<b>77.17</b>	<b>77.24</b>
	DINO [21]	ViT-Tiny	16	-	75.29	76.38	76.24
	Ours	ViT-Tiny	16	Mean	78.10	<b>82.51</b>	<b>82.41</b>
	Ours	ViT-Tiny	16	Sum	78.58	78.86	78.52
	Ours	ViT-Tiny	16	$\lambda = 0.9$	75.87	76.82	76.64
	Ours	ViT-Tiny	16	$\lambda = 0.8$	76.52	76.65	76.94
	Ours	ViT-Tiny	16	$\lambda = 0.5$	79.28	79.10	79.12
	Ours	ViT-Tiny	16	$\lambda = 0.2$	<b>79.65</b>	79.48	79.42
Ours	ViT-Tiny	16	$\lambda = 0.1$	79.06	79.36	79.04	

Table 7 The downstream tasks result comparison of our method with different configurations when pretrained on Cifar10. The proposed method is trained with ViT-Tiny as the backbone. The experiments are done with various configurations for loss function (patch-wise mean, patch-wise sum, and patch-wise  $\lambda$  with multiple values for  $\lambda$ ), and patch size 16. The mAP is reported for copy detection and image retrieval downstream tasks.

Pretraining Dataset	Method	Backbone	Patch size	Loss Function	Copy Detection	Image Retrieval	
						Oxford	Paris
Cifar10	Ours	ViT-Tiny	16	Mean	0.591	<b>M: 8.34, H: 1.63</b>	<b>M: 21.18, H: 5.11</b>
				Sum	0.534	M: 7.37, H: 1.47	M: 19.28, H: 4.26
				$\lambda = 0.9$	0.575	M: 6.35, H: 1.61	M: 17.71, H: 4.57
				$\lambda = 0.8$	0.585	M: 6.58, H: 1.52	M: 17.85, H: 4.57
				$\lambda = 0.5$	<b>0.592</b>	M: 6.72, H: 1.44	M: 17.51, H: 4.41
				$\lambda = 0.2$	0.580	M: 7.12, H: 1.63	M: 19.37, H: 4.68
				$\lambda = 0.1$	0.570	M: 6.90, H: 1.47	M: 20.15, H: 4.84

Table 8 The results comparison of our method with different configurations when pretrained on ImageNet-100. The proposed method is trained with ViT-Tiny, ViT-Small, and ViT-Base as the backbone. The experiments are done with patch-wise mean loss function, and patch sizes 16 and 8. Linear validation and KNN validation columns demonstrate the ImageNet-100 image classification accuracies

Pretraining Dataset	Method	Loss Function	Backbone	Patch size	Linear Validation	KNN Validation	
						(K=10)	(K=20)
ImageNet-100	Ours	Mean	ViT-Tiny	16	61.52	58.66	58.10
			ViT-Small	16	74.44	67.92	68.16
			ViT-Base	16	82.80	75.24	75.43
			ViT-Base	8	78.53	69.88	68.78

## 6. Conclusion

In this paper, we presented a local-global patch-wise representation learning algorithm that explored the benefits of considering patches within the self-supervised representation learning frameworks. The key idea was to pull representations of the local regions, e.g., patches as well as representations of the whole images across augmented views. This idea served as an inductive bias that could provide the model with useful insights into the details within the images. The alignment of corresponding patches among augmented views was achieved through the application of a novel, yet simple, patch-matching algorithm. Our exhaustive experimental assessments across varied datasets validate the effectiveness of our proposed approach. The local-global representation learning algorithm showcases its potential by elevating the state-of-the-art in self-supervised representation learning. This is evidenced by improvements in image classification accuracy: an increase of 1.38% on Cifar10, 1.34% on ImageNet-100, and 2.04% on ImageNet-1K. Furthermore, the method also demonstrated success in downstream tasks such as copy detection and image retrieval.

## REFERENCES

1. Wu, M., et al. *Conditional negative sampling for contrastive learning of visual representations*. in *International Conference on Learning Representations (ICLR)*. 2021.
2. Robinson, J., C.-Y. Chuang, S. Sra, and S. Jegelka. *Contrastive learning with hard negative samples*. in *International Conference on Learning Representations (ICLR)*. 2021.
3. Kotar, K., et al. *Contrasting contrastive self-supervised representation learning pipelines*. in *Proceedings of the IEEE/CVF International Conference on Computer Vision*. 2021.
4. Dwibedi, D., et al. *With a little help from my friends: Nearest-neighbor contrastive learning of visual representations*. in *Proceedings of the IEEE/CVF International Conference on Computer Vision*. 2021.
5. Xiong, Y., M. Ren, and R. Urtasun. *Loco: Local contrastive representation learning*. in *Advances in neural information processing systems (NeurIPS)*. 2020.
6. Tian, Y., D. Krishnan, and P. Isola. *Contrastive multiview coding*. in *European conference on computer vision (ECCV)*. 2020. Springer.
7. Kalantidis, Y., et al. *Hard negative mixing for contrastive learning*. in *Advances in Neural Information Processing Systems (NeurIPS)*. 2020.
8. He, K., et al. *Momentum Contrast for Unsupervised Visual Representation Learning*. in *IEEE/CVF Conference on Computer Vision and Pattern Recognition (CVPR)*. 2020.
9. Chen, T., S. Kornblith, M. Norouzi, and G. Hinton. *A simple framework for contrastive learning of visual representations*. in *International Conference on Machine Learning (ICML)*. 2020. PMLR.
10. Oord, A.v.d., Y. Li, and O. Vinyals. *Representation learning with contrastive predictive coding*. in *Advances in Neural Information Processing Systems (NeurIPS)*. 2018.
11. Gidaris, S., et al. *Obow: Online bag-of-visual-words generation for self-supervised learning*. in *Proceedings of the IEEE/CVF Conference on Computer Vision and Pattern Recognition (CVPR)*. 2021.
12. Yan, X., et al. *Clusterfit: Improving generalization of visual representations*. in *Proceedings of the IEEE/CVF Conference on Computer Vision and Pattern Recognition (CVPR)*. 2020.
13. Li, J., et al. *Prototypical Contrastive Learning of Unsupervised Representations*. in *International Conference on Learning Representations (ICLR)*. 2020.
14. Caron, M., et al. *Unsupervised learning of visual features by contrasting cluster assignments*. in *Advances in Neural Information Processing Systems (NeurIPS)*. 2020.
15. Caron, M., P. Bojanowski, A. Joulin, and M. Douze. *Deep clustering for unsupervised learning of visual features*. in *Proceedings of the European Conference on Computer Vision (ECCV)*. 2018.
16. Bardes, A., J. Ponce, and Y. LeCun. *Vicreg: Variance-invariance-covariance regularization for self-supervised learning*. in *International Conference on Learning Representations (ICLR)*. 2022.
17. Zhang, S., et al. *Zero-CL: Instance and Feature decorrelation for negative-free symmetric contrastive learning*. in *International Conference on Learning Representations (ICLR)*. 2021.
18. Zbontar, J., et al. *Barlow twins: Self-supervised learning via redundancy reduction*. in *International Conference on Machine Learning (ICML)*. 2021. PMLR.
19. Ermolov, A., A. Siarohin, E. Sangineto, and N. Sebe. *Whitening for self-supervised representation learning*. in *International Conference on Machine Learning (ICML)*. 2021. PMLR.
20. Chen, X. and K. He. *Exploring simple siamese representation learning*. in *Proceedings of the IEEE/CVF Conference on Computer Vision and Pattern Recognition (CVPR)*. 2021.
21. Caron, M., et al. *Emerging Properties in Self-Supervised Vision Transformers*. in *Proceedings of the IEEE International Conference on Computer Vision (ICCV)*. 2021.
22. Azabou, M., et al., *Mine your own view: Self-supervised learning through across-sample prediction*. CoRR, 2021. **abs/2102.10106**.
23. Grill, J.-B., et al. *Bootstrap your own latent: A new approach to self-supervised learning*. in *Advances in Neural Information Processing Systems (NeurIPS)*. 2020.
24. Bachman, P., R.D. Hjelm, and W. Buchwalter. *Learning representations by maximizing mutual information across views*. in *Advances in Neural Information Processing Systems (NeurIPS)*. 2019.
25. Yun, S., H. Lee, J. Kim, and J. Shin. *Patch-Level Representation Learning for Self-Supervised Vision Transformers*. in *Proceedings of the IEEE/CVF Conference on Computer Vision and Pattern Recognition (CVPR)*. 2022.
26. Li, C., et al. *Efficient self-supervised vision transformers for representation learning*. in *Proceedings of the International Conference on Learning Representations (ICLR)*. 2022.
27. Zhang, T., et al. *Leverage your local and global representations: A new self-supervised learning strategy*. in *Proceedings of the IEEE/CVF Conference on Computer Vision and Pattern Recognition*. 2022.
28. Chen, T., et al. *Big self-supervised models are strong semi-supervised learners*. in *Advances in Neural Information Processing Systems (NeurIPS)*. 2020.
29. Chen, X., H. Fan, R. Girshick, and K. He. *Improved baselines with momentum contrastive learning*. CoRR, 2020. **abs/2003.04297**.
30. Chen, X., S. Xie, and K. He. *An empirical study of training self-supervised vision transformers*. in *Proceedings of the IEEE/CVF Conference on Computer Vision and Pattern Recognition (CVPR)*. 2021.

31. Jang, J., et al. *Self-distilled self-supervised representation learning*. in *Proceedings of the IEEE/CVF Winter Conference on Applications of Computer Vision*. 2023.
32. Tian, Y., et al. *What makes for good views for contrastive learning?* in *Advances in Neural Information Processing Systems (NeurIPS)*. 2020.
33. Peng, X., et al. *Crafting better contrastive views for siamese representation learning*. in *Proceedings of the IEEE/CVF Conference on Computer Vision and Pattern Recognition (CVPR)*. 2022.
34. Wang, W., et al. *Instance-wise Hard Negative Example Generation for Contrastive Learning in Unpaired Image-to-Image Translation*. in *Proceedings of the IEEE/CVF Conference on Computer Vision and Pattern Recognition (CVPR)*. 2021.
35. Huynh, T., et al. *Boosting contrastive self-supervised learning with false negative cancellation*. in *Proceedings of the IEEE/CVF winter conference on applications of computer vision*. 2022.
36. Long, X., H. Du, and Y. Li, *Two momentum contrast in triplet for unsupervised visual representation learning*. *Multimedia Tools and Applications*, 2023: p. 1-14.
37. Vasudeva, K., A. Dubey, and S. Chandran, *SCL-FExR: supervised contrastive learning approach for facial expression Recognition*. *Multimedia Tools and Applications*, 2023: p. 1-21.
38. Agilandeewari, L. and S.D. Meena, *SWIN transformer based contrastive self-supervised learning for animal detection and classification*. *Multimedia Tools and Applications*, 2023. **82(7)**: p. 10445-10470.
39. Xie, J., R. Girshick, and A. Farhadi. *Unsupervised deep embedding for clustering analysis*. in *International Conference on Machine Learning (ICML)*. 2016. PMLR.
40. Mo, S., Z. Sun, and C. Li. *Multi-level contrastive learning for self-supervised vision transformers*. in *Proceedings of the IEEE/CVF Winter Conference on Applications of Computer Vision*. 2023.
41. Hsieh, C.-Y., C.-J. Chang, F.-E. Yang, and Y.-C.F. Wang. *Self-Supervised Pyramid Representation Learning for Multi-Label Visual Analysis and Beyond*. in *Proceedings of the IEEE/CVF Winter Conference on Applications of Computer Vision*. 2023.
42. Moon, S., et al. *An Embedding-Dynamic Approach to Self-Supervised Learning*. in *Proceedings of the IEEE/CVF Winter Conference on Applications of Computer Vision*. 2023.
43. Jing, L., P. Vincent, Y. LeCun, and Y. Tian, *Understanding dimensional collapse in contrastive self-supervised learning*. arXiv preprint arXiv:2110.09348, 2021.
44. Zhang, S., et al. *Align Representations with Base: A New Approach to Self-Supervised Learning*. in *Proceedings of the IEEE/CVF Conference on Computer Vision and Pattern Recognition (CVPR)*. 2022.
45. Wang, F., et al., *Self-Supervised Learning by Estimating Twin Class Distributions*. *CoRR*, 2021. **abs/2110.07402**.
46. Amrani, E. and A. Bronstein. *Self-Supervised Classification Network*. in *European Conference on Computer Vision (ECCV)*. 2022.